The Astrophysical Journal, 808:51 (23pp), 2015 July 20 doi:10.1088/0004-637X/808/1/51

THE *HUBBLE SPACE TELESCOPE* UV LEGACY SURVEY OF GALACTIC GLOBULAR CLUSTERS. III. A QUINTUPLE STELLAR POPULATION IN NGC 2808*

A. P. Milone[1], A. F. Marino[1], G. Piotto[2,3], A. Renzini[3], L. R. Bedin[3], J. Anderson[4], S. Cassisi[5], F. D'Antona[6], A. Bellini[4], H. Jerjen[1], A. Pietrinferni[5], and P. Ventura[6]

[1] Research School of Astronomy and Astrophysics, The Australian National University, Cotter Road, Weston, ACT, 2611, Australia
[2] Istituto Nazionale di Astrofisica—Osservatorio Astronomico di Padova, Vicolo dell'Osservatorio 5, Padova, IT-35122, Italy
[3] Dipartimento di Fisica e Astronomia "Galileo Galilei," Univ. di Padova, Vicolo dell'Osservatorio 3, Padova, IT-35122, Italy
[4] Space Telescope Science Institute, 3800 San Martin Drive, Baltimore, MD 21218, USA
[5] Istituto Nazionale di Astrofisica—Osservatorio Astronomico di Teramo, Via Mentore Maggini s.n.c., I-64100 Teramo, Italy
[6] Istituto Nazionale di Astrofisica—Osservatorio Astronomico di Roma, Via Frascati 33, I-00040 Monteporzio Catone, Roma, Italy
Received 2015 March 5; accepted 2015 May 21; published 2015 July 17

ABSTRACT

In this study we present the first results from multi-wavelength *Hubble Space Telescope* (*HST*) observations of the Galactic globular cluster (GC) NGC 2808 as an extension of the *Hubble Space Telescope UV Legacy Survey of Galactic GCs* (GO-13297 and previous proprietary and *HST* archive data). Our analysis allowed us to disclose a multiple-stellar-population phenomenon in NGC 2808 even more complex than previously thought. We have separated at least five different populations along the main sequence and the red giant branch (RGB), which we name A, B, C, D, and E (though an even finer subdivision may be suggested by the data). We identified the RGB bump in four out of the five RGBs. To explore the origin of this complex color–magnitude diagram, we have combined our multi-wavelength *HST* photometry with synthetic spectra, generated by assuming different chemical compositions. The comparison of observed colors with synthetic spectra suggests that the five stellar populations have different contents of light elements and helium. Specifically, if we assume that NGC 2808 is homogeneous in [Fe/H] (as suggested by spectroscopy for Populations B, C, D, E, but lacking for Population A) and that population A has a primordial helium abundance, we find that populations B, C, D, E are enhanced in helium by $\Delta Y \sim 0.03$, 0.03, 0.08, 0.13, respectively. We obtain similar results by comparing the magnitude of the RGB bumps with models. Planned spectroscopic observations will test whether Population A also has the same metallicity, or whether its photometric differences with Population B can be ascribed to small [Fe/H] and [O/H] differences rather than to helium.

Key words: globular clusters: individual (NGC 2808) – stars: Population II

1. INTRODUCTION

Recent studies, based on multi-wavelength photometry, have revealed that the color–magnitude diagram (CMD) of all Galactic globular clusters (GCs) so far explored (Piotto et al. 2015, hereafter Paper I) is made of distinct sequences of stars that can be traced continuously from the bottom of the main sequence (MS) up to the tip of the red giant branch (RGB) and through the horizontal branch (HB) and the asymptotic giant branch (AGB). These sequences stand in contrast to the traditional view of GCs as the best example of simple stellar populations, i.e., made of stars born all at the same time and with the same chemical composition, confirming previous findings of CN variations in MS and RGB stars (Cannon et al. 1998; Grundahl et al. 1998; Grundahl 1999).

The *Hubble Space Telescope UV Legacy Survey of Galactic GCs* is a *Hubble Space Telescope* (*HST*) project to observe 54 GCs through the filters F275W, F336W, F438W of the Wide Field Camera 3 (WFC3) on board *HST* (see Paper I). This data set complements the existing F606W and F814W photometry from the Advanced Camera for Surveys (GO-10775, Sarajedini et al. 2007; Anderson et al. 2008) and is specifically designed to map multiple stellar populations in GCs.

NGC 2808 is one of the most intriguing Galactic GCs in the context of multiple stellar populations. It hosts a multimodal MS (D'Antona et al. 2005; Piotto et al. 2007; Milone et al. 2012a; Paper I), and exhibits a multimodal HB (Sosin et al. 1997; Bedin et al. 2000; Dalessandro et al. 2011) and RGB (Lee et al. 2009; Monelli et al. 2013; Paper I). Spectroscopy has shown star-to-star variations of several light elements and lithium, and an extended Na–O anticorrelation (Norris & Smith 1983; Carretta et al. 2006, 2010; Gratton et al. 2011; Carretta 2014; Marino et al. 2014; D'Orazi et al. 2015). These observations have been interpreted with multiple populations of stars with different helium abundance, from primordial abundance, $Y \sim 0.246$, up to extreme enhancement, $Y \sim 0.38$ (e.g., D'Antona et al. 2002, 2005; Piotto et al. 2007; Milone et al. 2012a). Evidence of helium enhancement in NGC 2808 has also been confirmed by direct measurements of helium-rich stars along the RGB and the HB (Pasquini et al. 2011; Marino et al. 2014).

While previous studies on multiple MSs in NGC 2808 were based on visual or near-infrared photometry, in this paper we extend the study to the ultraviolet. The ultraviolet region of the spectrum is indeed very powerful in the study of multiple stellar populations with different chemical composition. Molecular bands, such as OH, NH, CH, and CN, affect the ultraviolet and blue wavelengths, which are thus sensitive to populations with different C, N, and O compositions (Milone et al. 2012b; Paper I).

In this paper we use multi-wavelength ultraviolet and visual photometry (from Paper I) of stars in a field centered on NGC 2808 in order to identify multiple stellar populations in

* Based on observations with the NASA/ESA *Hubble Space Telescope*, obtained at the Space Telescope Science Institute, which is operated by AURA, Inc., under NASA contract NAS 5-26555.

Table 1
List of the Data Sets Used in This Paper

Instrument	Date	$N \times$ Exposure Time	Filter	Program	PI
ACS/WFC	2004 May 5	6 × 340 s	F475W	9899	G.Piotto
ACS/WFC	2006 Aug 9 and Nov 2	20 s + 2 × 350 s + 2 × 360 s	F475W	10922	G. Piotto
ACS/WFC	2006 Aug 9 and Nov 1	10 s + 3 × 350 s + 3 × 360 s	F814W	10922	G. Piotto
ACS/WFC	2006 Jan 1	23 s + 5 × 360 s	F606W	10775	A. Sarajedini
ACS/WFC	2006 Jan 1	23 s + 5 × 370 s	F814W	10775	A. Sarajedini
WFC3/UVIS	2013 Sep 8–9	12 × 985 s	F275W	12605	G. Piotto
WFC3/UVIS	2013 Sep 8–9	6 × 650 s	F336W	12605	G. Piotto
WFC3/UVIS	2013 Sep 8–9	6 × 97 s	F438W	12605	G. Piotto

the CMDs. The behavior of multiple sequences in appropriate CMDs made with different combinations of colors and magnitudes will provide unique information on the helium and light-element content of the different stellar populations of this extreme GC.

The paper is organized as follows. In Section 2 we present the data and the data reduction. In Section 3 we analyze the CMDs and investigate multiple populations along the RGB and the MS. Helium and C, N, O abundances of the stellar populations are inferred in Section 4 from multiple MS and RGB locations in the CMD. The bumps of multiple RGBs of NGC 2808 are analyzed in Section 5, while Sections 7 and 8 are dedicated to the HB and the AGB. A discussion will follow in Section 9.

2. DATA AND DATA REDUCTION

In our study of NGC 2808 we have used archival and proprietary images taken with the Wide Field Channel of the Advanced Camera for Surveys (WFC/ACS) and the Ultraviolet and Visual Channel of the Wide Field Camera 3 (UVIS/WFC3) on board the *Hubble Space Telescope* (*HST*). Table 1 summarizes the data sets.

The poor charge-transfer efficiency (CTE) in the UVIS/WFC3 and ACS/WFC images has been corrected by following the recipe of Anderson & Bedin (2010). Photometry and astrometry of UVIS/WFC3 images were already presented in Paper I and were obtained with *img2xym_UVIS_09* × 10, which is a software package presented by Bellini et al. (2010) and mostly adapted from *img2xym_WFI* (Anderson et al. 2006). We used pixel-area and geometric-distortion corrections from Bellini & Bedin (2009) and Bellini et al. (2011). The photometry has been calibrated as in Bedin et al. (2005), and uses the encircled energy and the zero points available at the STScI web page. We used the photometric and astrometric catalogs from WFC/ACS data published by Anderson et al. (2008), Sarajedini et al. (2007), Milone et al. (2012a), and Piotto et al. (2007), which were obtained from GO-9899, GO-10922, and GO-10775 WFC/ACS data.

In order to investigate multiple stellar populations in NGC 2808 we are interested in stars for which high-accuracy photometry is available. The stellar catalogs were purged of stars that are poorly measured by using the procedure described by Milone et al. (2009) and based on the quality indexes provided by our software (see Anderson et al. 2006, 2008). Photometry has been corrected for differential reddening following the recipe in Milone et al. (2012a).

3. THE MULTIPLE PHOTOMETRIC COMPONENTS ALONG THE CMD OF NGC 2808

As already discussed in Section 1, previous studies based on ACS/*HST* and ground-based photometry have shown that NGC 2808 has at least a triple MS (Piotto et al. 2007; Milone et al. 2012a) and a broadened RGB (Lee et al. 2009; Monelli et al. 2013; Paper I). An inspection of the large number of CMDs that we derived from six-band photometry immediately reveals that NGC 2808 is even more complex than initially thought, and hosts more than three stellar populations.

A visual example of its complexity is provided by the CMDs in Figure 1. This figure shows several diagrams, after the quality selection and the differential-reddening correction described in the previous section were applied. To derive some of the diagrams of Figure 1 we have defined the pseudo-magnitudes $m_{\rm F336W,F275W,F814W} = (m_{\rm F336W} - m_{\rm F275W} + m_{\rm F814W})$ and $m_{\rm F275W,F336W,F814W} = (m_{\rm F275W} - m_{\rm F336W} + m_{\rm F814W})$, which allow us to better distinguish multiple sequences along the RGB and the MS. An inspection of these CMDs immediately suggests that both the RGB and MS are made of multiple sequences, which look discrete in the $m_{\rm F275W}$ versus $m_{\rm F275W} - m_{\rm F814W}$, $m_{\rm F275W,F336W,F814W}$ versus $m_{\rm F275W} - m_{\rm F336W}$, and $m_{\rm F336W,F275W,F814W}$ versus $2\,m_{\rm F275W} - m_{\rm F438W} - m_{\rm F814W}$ diagrams. We also observe a widely spread subgiant branch (SGB) in the $m_{\rm F275W}$ versus $m_{\rm F336W} - m_{\rm F438W}$ CMD as shown in the upper-right inset of Figure 1. In the following we discuss the observed morphology of the CMD at various evolutionary stages: the RGB, MS, AGB, and HB.

3.1. The Quintuple RGB

Along the RGB, the behavior of multiple populations dramatically changes from one CMD to another. In order to investigate this phenomenon, in Figure 2 we compare the $m_{\rm F814W}$ versus $m_{\rm F275W} - m_{\rm F814W}$ CMD of RGB stars (upper-left panel) and of the $m_{\rm F814W}$ versus $m_{\rm F336W} - m_{\rm F438W}$ CMD (upper-right panel). The insets show the Hess diagrams for stars in the magnitude interval with $14.5 < m_{\rm F814W} < 17.7$ where multiple RGBs are clearly visible. Multiple stellar populations manifest themselves as four separate sequences in $m_{\rm F275W} - m_{\rm F814W}$, while the $m_{\rm F336W} - m_{\rm F438W}$ color distribution is more broadened and only two RGBs can be recognized.

In order to compare the two CMDs, we used the procedure introduced by Milone et al. (2015, hereafter Paper II) in their study of multiple populations in M2, and illustrated in Figure 2 for the case of NGC 2808. For that purpose, we drew two fiducial lines in each CMD. The blue and red fiducials mark the bluest and reddest envelopes of the RGB, respectively, and have been derived as follows. We have divided the RGB portion with $m_{\rm F814W} > 14.8$ into intervals of 0.2 magnitudes in

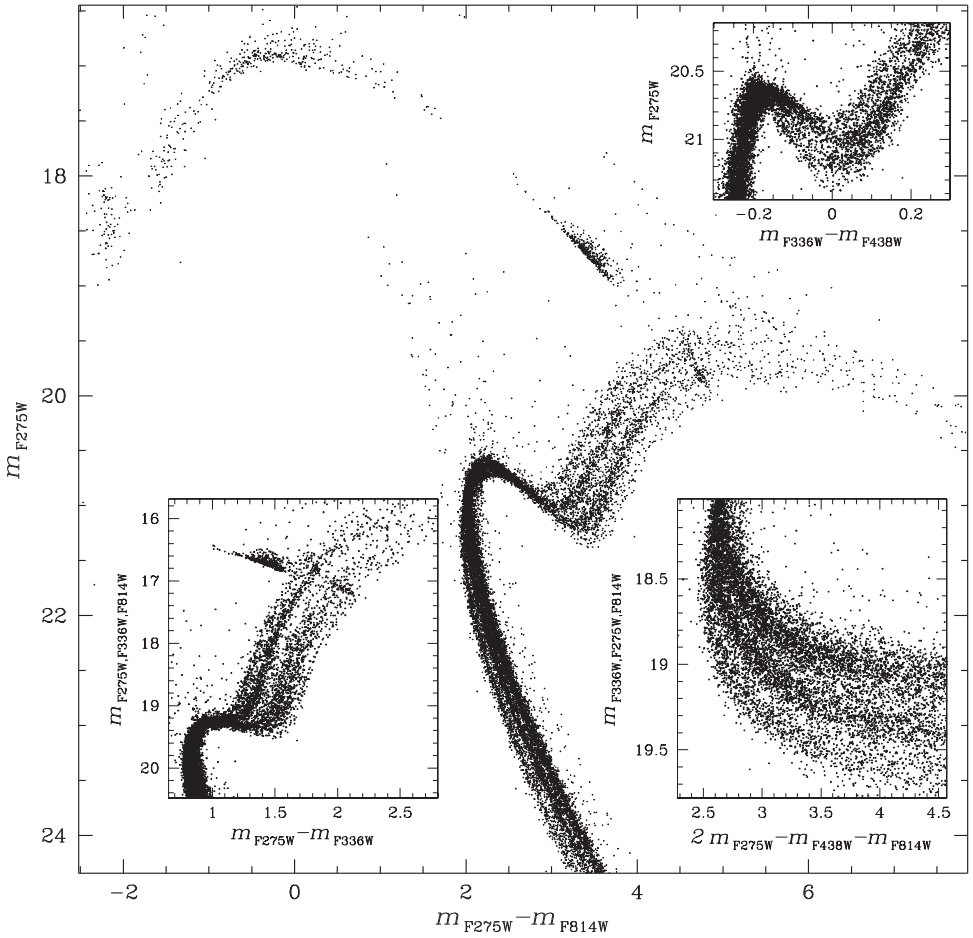

Figure 1. m_{F275W} vs. $m_{F275W} - m_{F814W}$ CMD of NGC 2808. The $m_{F275W,F336W,F814W}$ against $m_{F275W} - m_{F336W}$ (bottom-left inset), $m_{F336W,F275W,F814W}$ against $2\,m_{F275W} - m_{F438W} - m_{F814W}$ (bottom-right inset), and m_{F275W} vs. $m_{F336W} - m_{F438W}$ (upper-right inset) diagrams highlight multiple sequences along the RGB, the MS, and the SGB, respectively.

the F814W band. For each interval, we have determined the 4th and the 96th percentiles of the $m_{F275W} - m_{F814W}$ or $m_{F336W} - m_{F438W}$ color distribution and the median m_{F814W} magnitude. The points corresponding to the 4th percentile and the median magnitude have been interpolated with a cubic spline to derive the blue fiducial, while the red fiducial has been similarly derived. Due to small number statistics it is not possible to infer robust estimates of the RGB envelopes with this method at brighter luminosities. Therefore, the portions of the blue and red lines in the magnitude interval with $m_{F814W} < 14.8$ have been derived by hand by trying to follow the blue and red envelopes of the RGB, respectively.

Then we have verticalized the two CMDs in such a way that the blue and red fiducials translate into vertical lines with abscissa −1 and 0, respectively. To do this, we defined for each star: $\Delta^N_X = [(X - X_{\rm blue\ fiducial})/(X_{\rm red\ fiducial} - X_{\rm blue\ fiducial})] - 1$ where $X = (m_{F275W} - m_{F814W})$, $(m_{F336W} - m_{F438W})$ and $X_{\rm blue\ fiducial}$ and $X_{\rm red\ fiducial}$ are obtained by subtracting the color of the fiducial at the corresponding F814W magnitude from the color of each star. The verticalized m_{F814W} versus $\Delta^N_{F275W,F814W}$ and m_{F814W} versus $\Delta^N_{F336W,F438W}$ diagrams are plotted in the lower-left panels of Figure 2. RGB stars in NGC 2808 are clustered around distinct values of $\Delta^N_{F336W,F438W}$ and $\Delta^N_{F275W,F814W}$, as shown in the bottom-right panel of Figure 2.

As previously discussed by Anderson et al. (2008, see their Section 8.1), F814W photometry of bright RGB stars is less accurate than that of the remaining RGB stars because it has been derived by using saturated stars (see Anderson et al. 2008 for details). Indeed, multiple sequences are less evident above the gray dashed lines in the lower-left panels of Figure 2. Dashed lines are placed at $m_{F814W} = 14.68$. To investigate whether the distinct sequences can also be detected along the brightest RGB segment or not, we have marked stars with $m_{F814W} < 14.68$ with red dots in the lower panels of Figure 2. The distribution of these bright RGB stars on the $\Delta^N_{F336W,F438W}$ versus $\Delta^N_{F275W,F814W}$ plot shows that they share the same color distribution as the fainter RGB stars.

To further investigate the stellar populations along the RGB, in the upper-right panel of Figure 3 we plot the $\Delta^N_{F336W,F438W}$ versus $\Delta^N_{F275W,F814W}$ Hess diagram. At least five main clumps of RGB stars are clearly visible. These are selected by eye and designated A, B, C, D, and E and are colored green, orange, yellow, cyan, and blue, respectively (see the lower-left panel). These color codes will be consistently used in the paper. RGB-A–E contain $(5.8 \pm 0.5)\%$, $(17.4 \pm 0.9)\%$, $(26.4 \pm 1.2)\%$, $(31.3 \pm 1.3)\%$, and $(19.1 \pm 1.0)\%$ of the total number of RGB stars with $12.25 < m_{F814W} < 17.70$, respectively. In Section 3.3 we show that populations A–E have different chemical composition.

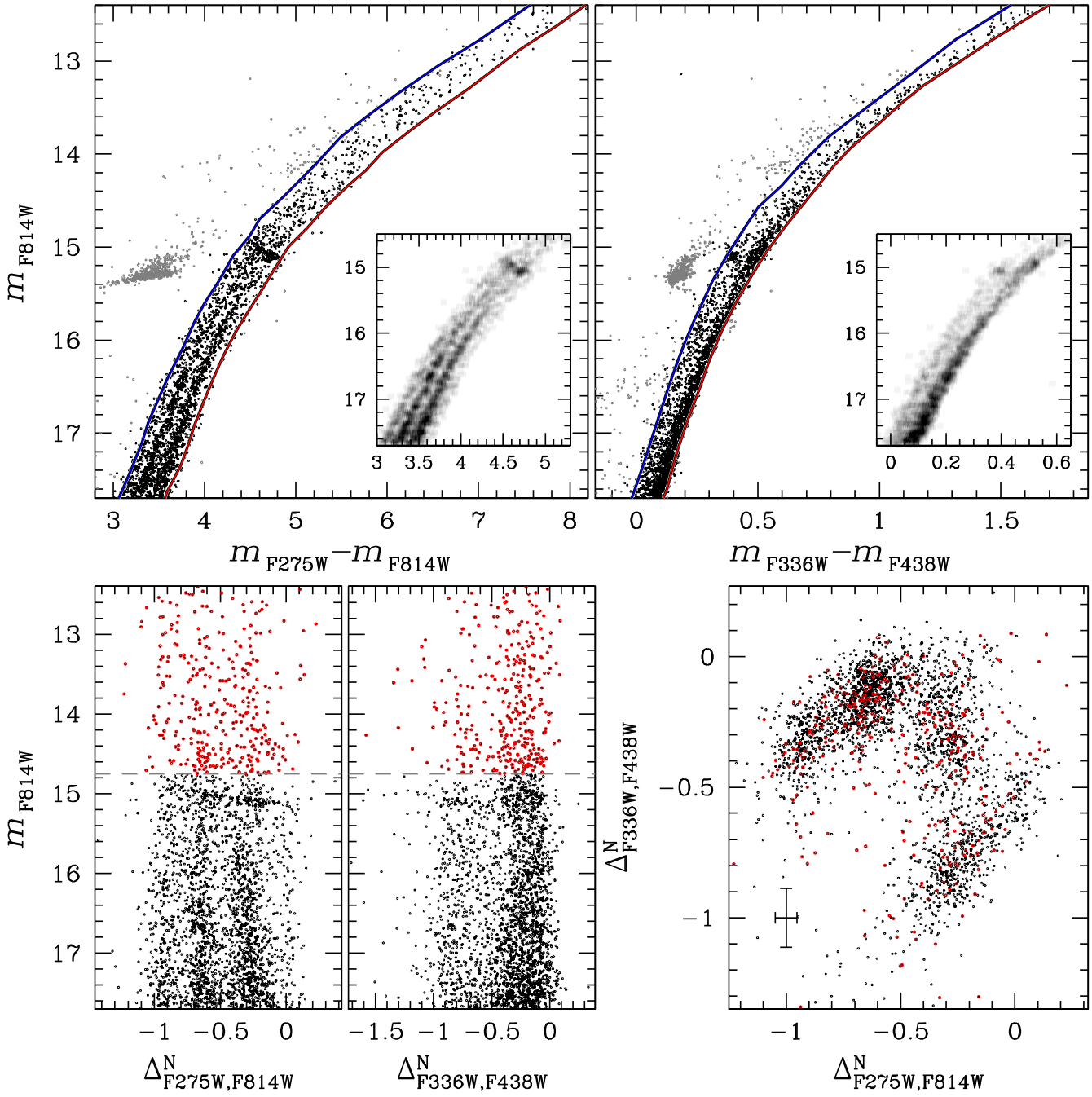

Figure 2. Upper panels: zoom of the m_{F814W} vs. $m_{F275W} - m_{F814W}$ (left) and of the m_{F814W} vs. $m_{F336W} - m_{F438W}$ (right) CMD of NGC 2808 around the RGB. Only RGB stars colored black are used in the following analysis. Red and blue lines are the fiducials adopted to verticalize the RGB (see text for details). The insets show the Hess diagram for RGB stars with $12.25 < m_{F814W} < 17.7$. Lower panels: verticalized m_{F814W} vs. $\Delta^N_{F275W,F814W}$ (left) and m_{F814W} vs. $\Delta^N_{F336W,F438W}$ (middle) diagrams for RGB stars. $\Delta^N_{F336W,F438W}$ is plotted against $\Delta^N_{F275W,F814W}$ in the lower-right panel. RGB stars with $m_{F814W} < 14.68$ are colored red.

The $\Delta^N_{F275W,F814W}$ and $\Delta^N_{F336W,F438W}$ distributions of RGB stars are shown in the upper-left and lower-right panel of Figure 3, respectively. Black histograms represent the whole sample of RGB stars shown in the lower-left panel, while the distributions of the five distinct RGBs are plotted with shaded colored histograms. The $\Delta^N_{F275W,F814W}$ and $\Delta^N_{F336W,F438W}$ distributions exhibit significant differences. The histogram distribution of $\Delta_{F275W,F814W}$ clearly shows three main peaks at $\Delta^N_{F275W,F814W} \sim -0.9$, –0.6, and –0.3. The first and second clumps are mainly composed of population-E and population-D stars, respectively, while the third peak is a mix of both population-B and population-C stars. A less populous peak, corresponding to population A, is located at $\Delta^N_{F275W,F814W} \sim 0.0$. In contrast, the $\Delta^N_{F336W,F438W}$ distribution looks bimodal. Most of the stars of populations C, D, and E have $\Delta^N_{F336W,F438W} > -0.5$ and determine the main peak at $\Delta^N_{F336W,F438W} \sim -0.2$. A second peak, mostly composed of population-B stars, is located around $\Delta^N_{F336W,F438W} \sim -0.8$.

In addition we note that:

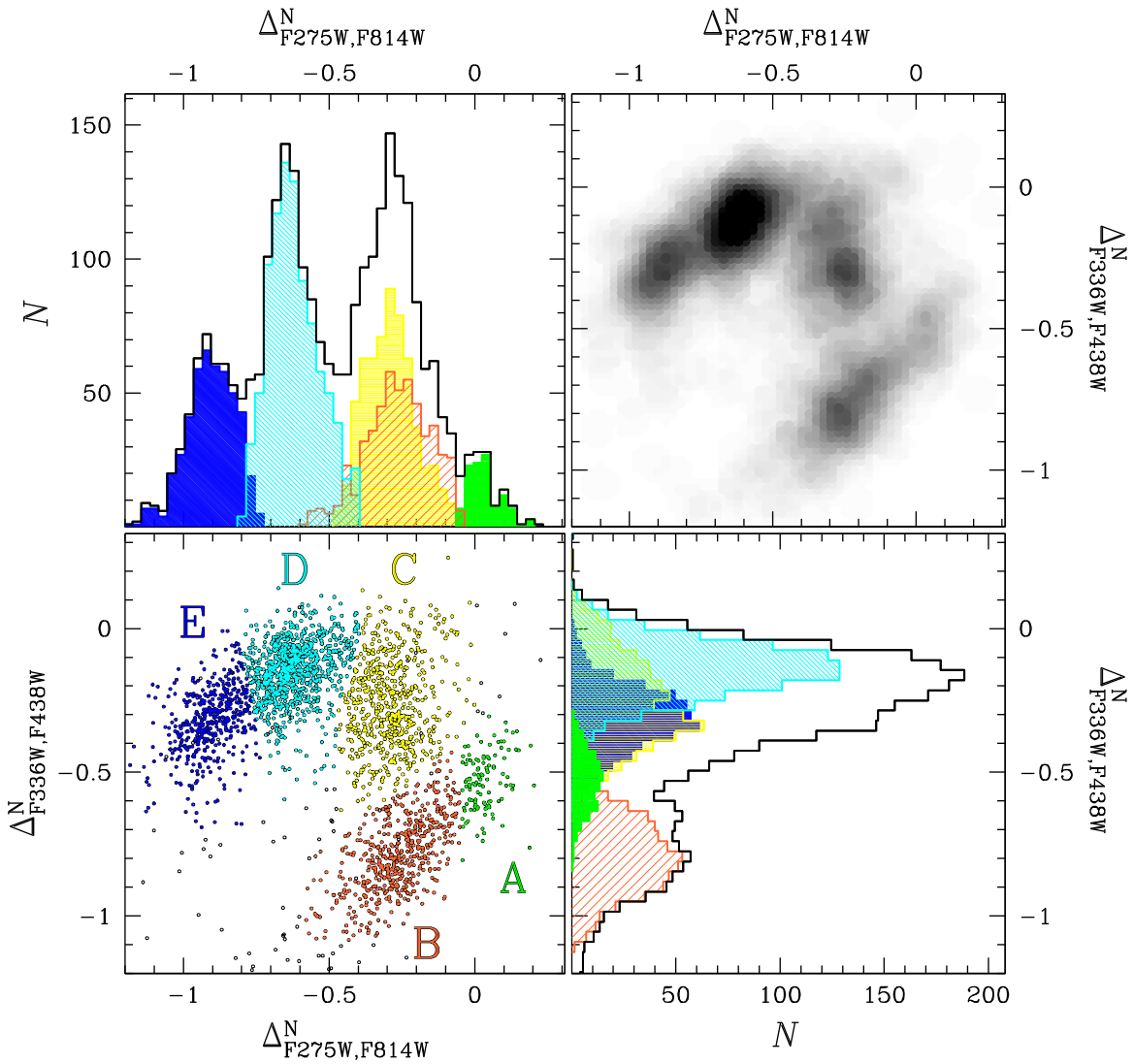

Figure 3. Reproduction of the $\Delta_{F336W,F438W}$ vs. $\Delta_{F275W,F814W}$ diagram of Figure 2. Stars in the groups A, B, C, D, and E are colored green, orange, yellow, cyan, and blue, respectively (lower-left panel). The corresponding Hess diagram is plotted in the upper-right panel. The histograms of the normalized $\Delta_{F275W,F814W}$ and $\Delta_{F336W,F438W}$ distributions for all the analyzed RGB stars are plotted in black in the upper-left and lower-right panels, respectively. The shaded colored histograms show the distributions for each of the five populations defined in the lower-left panel.

1. Populations B and C are mixed in the $\Delta^{N}_{F275W,F814W}$ color range while they have distinct $\Delta^{N}_{F336W,F438W}$ values, with population-B stars having also smaller $\Delta^{N}_{F336W,F438W}$ values.
2. Population-A stars have larger $\Delta^{N}_{F275W,F814W}$ than both populations B and C. The color order is different in $\Delta_{F336W,F438W}$, where the histogram of population-A stars is located between the histograms of populations B and C.
3. Since the analyzed RGB stars cover the same F814W magnitude interval and have similar m_{F336W} and m_{F438W} magnitudes, their photometric errors are similar. We note that the $\Delta^{N}_{F336W,F438W}$ spread for populations B and C ($\sigma^{N,B}_{\Delta F336W,F438W} = 0.13 \pm 0.01$ and $\sigma^{N,C}_{\Delta F336W,F438W} = 0.16 \pm 0.01$) is significantly larger than the spread observed for stars of populations A, D, and E ($\sigma^{N,D}_{\Delta F336W,F438W} = 0.10 \pm 0.02$, $\sigma^{N,D}_{\Delta F336W,F438W} = 0.10 \pm 0.01$, and $\sigma^{N,E}_{\Delta F336W,F438W} = 0.10 \pm 0.01$). This fact indicates that the $m_{F336W} - m_{F438W}$ color spread observed for populations B and C is, in part, intrinsic and that both group B and group C are not simple stellar populations. In fact, a visual inspection of the Hess diagram of Figure 3 suggests that both groups consist of two clumps of stars that are clustered around $\Delta^{N}_{F336W,F438W} \sim -0.85, -0.65$ (group B) and $-0.2, -0.1$ (group C), thus suggesting that stars in both groups B and C do not have homogeneous chemical composition. More data are needed to establish whether these clumps correspond to distinct stellar populations.

The causes of the "discreteness" of multiple populations as observed in the CMD and two-color diagram of some GCs are still unknown, and have been associated with distinct bursts of star formation (see Renzini 2008 for a critical discussion). The referee has pointed out that the distinct bumps in the diagrams of Figure 3 could indicate that some abundances are favored over the others and suggested a possible connection between the abundances of stars in the distinct clumps of NGC 2808 and

metal mixtures that are consistent with equilibrium CN or equilibrium ON cycling. While this hypothesis deserves some investigation that is beyond the purposes of our paper, we emphasize that the evidence of discrete populations in NGC 2808 provides a strong constraint for any model of formation and evolution of stellar populations in GCs.

At the request of the referee and of the Statistical Editor of this journal, Prof. Eric Feigelson, we have used the Mcluster CRAN package in the public-domain R statistical software system to estimate how many groups are statistically significant. This package is based on the method described in detail in the monograph "*Finite Mixture Models*" by McLachlan & Peel (2000). It performs the maximum likelihood fits to different numbers of stellar groups, and evaluates the number of groups by the Bayesian information criterion (BIC) penalized likelihood measure for model complexity.

To do this it uses several different assumptions about shape and size of the different populations in a plot such as that shown in Figure 3. For each shape and size that we adopted for the populations, we assumed a number, N, of stellar populations from 1 to 20 and estimated a BIC for each combination. We obtain the best BIC value (BIC = 1784) for $N = 6$ under the assumption that the stellar populations have equal shapes but variable volume and orientations (VEV). The second most likely explanation (BIC = 1778) corresponds to $N = 6$ but assumes equal shape, VEV. The third best value (BIC = 1776) corresponds to a VEV assumption and seven stellar populations. All the three best models assume ellipsoidal distributions.

Results from this statistical analysis support the conclusion that our observations of NGC 2808 are consistent with more than five groups of stars, and that group C hosts more than one stellar population. The third best BIC value suggests that also the group B is not consistent with a simple population. Thus, the statistical analysis confirms what was already pretty evident from a purely visual inspection of the plots. In the following, we will study the five most evident stellar populations, A–E.

3.2. Multiple Populations Along the MS

The MS of NGC 2808 exhibits different patterns in CMDs based on different photometric bands, in close analogy with what we observe along the RGB. This is shown in the upper panels of Figure 4 where we compare the $m_{\rm F814W}$ versus $m_{\rm F275W} - m_{\rm F814W}$ (left panel) and the $m_{\rm F814W}$ versus $m_{\rm F336W} - m_{\rm F438W}$ (right panel) CMDs of MS stars with $19.6 < m_{\rm F814W} < 20.7$. The MS looks discrete in $m_{\rm F275W} - m_{\rm F814W}$ with three distinct components, in contrast with the $m_{\rm F336W} - m_{\rm F438W}$ color distribution, which looks broadened without any evidence for discrete sequences.

In order to identify the different stellar populations, we have verticalized the MSs by following the same recipe as introduced in Section 3.1 for the RGB, and using the fiducial lines drawn in the upper-panel CMDs. The $m_{\rm F814W}$ versus $\Delta^{\rm N}_{\rm F275W,F814W}$ and the $m_{\rm F814W}$ versus $\Delta^{\rm N}_{\rm F336W,F438W}$ diagrams are plotted in the lower-left and lower-middle panels, while the lower-right panel shows $\Delta^{\rm N}_{\rm F336W,F438W}$ against $\Delta^{\rm N}_{\rm F275W,F814W}$.

The pseudo-color $C_{\rm F275W,F336W,F438W} = (m_{\rm F275W} - m_{\rm F336W}) - (m_{\rm F336W} - m_{\rm F438W})$ defined by Milone et al. (2013) is another valuable tool to identify multiple populations in GCs. To better distinguish the distinct MSs and RGBs of NGC 2808 we show in the left panel of Figure 5 the $m_{\rm F814W}$ versus $C_{\rm F275W,F336W,F438W}$ pseudo CMD for this cluster. The red and the blue lines superimposed on this diagram are the envelopes of the MS and the RGB, and have been determined with the same procedure as in Section 3.1. These two fiducials are used to verticalize the MS and the RGB. The verticalized $m_{\rm F814W}$ versus $\Delta^{\rm N}_{CF275W,F336W,F438W}$ diagram for RGB and MS stars is plotted in the middle panels. An inspection of these figures reveals that three distinct sequences are present along the RGB, while only two MSs are visible. In the right panels of Figure 5 we plot $\Delta^{\rm N}_{\rm F275W,F814W}$ against $\Delta^{\rm N}_{CF275W,F336W,F438W}$ for RGB (upper panel) and MS stars (lower panel).

In order to identify stellar populations along the MS, we exploit the $\Delta^{\rm N}_{\rm F336W,F438W}$ versus $\Delta^{\rm N}_{\rm F275W,F814W}$ diagram and the $\Delta^{\rm N}_{\rm F275W,F336W,F438W}$ versus $\Delta^{\rm N}_{\rm F275W,F814W}$ Hess diagram shown in the lower-left and upper-right panels of Figure 6, respectively. The distribution of MS stars in this plane is similar to that observed for the RGB, as better highlighted by the Hess diagram in the upper-right panel Figure 6. There are at least four groups of MS stars that we denote B, C, D, and E, and color orange, yellow, cyan, and blue, in the bottom-left and rightmost panels, in close analogy with what was done for the RGB. Colors introduced in this figure will be used consistently hereafter. It is noticeable that the separation among the four groups is less clear for the MS than in the case of the RGB. This could be due to fact that colors of these relatively hot MS stars are less sensitive to light-element variations than the RGB. Indeed we have shown in our previous papers that the color difference between multiple MSs and RGBs is due, apart from helium, to different strengths of the molecular bands between the distinct populations of stars (Marino et al. 2008; Milone et al. 2012a). In particular, the OH band and the CH G-band, which are stronger in the stellar population with the same chemical composition as halo field stars of the same metallicity, mainly fall in the F275W and the F438W bands, respectively, while the NH band, which is weaker in stars of this population, mainly affects the F336W magnitude. Population A is not clearly distinguishable, even if a stellar overdensity can be recognized in the Hess diagram at $(\Delta^{\rm N}_{\rm F275W,F814W}; \Delta^{\rm N}_{\rm F336W,F438W}) \sim (0.0; -0.5)$. We tentatively associate these stars with population A and color them green in the lower-left panel. In the upper-middle and upper-right panels of Figure 6 we compare the $\Delta^{\rm N}_{\rm F275W,F336W,F438W}$ versus $\Delta^{\rm N}_{\rm F275W,F814W}$ Hess diagrams for RGB and MS stars, while, in the corresponding lower panels, we show the position of Populations A–E in this plane.

In order to further investigate whether MS-A stars correspond to a distinct stellar population or whether their position in the $\Delta^{\rm N}_{\rm F275W,F814W}$ versus $\Delta^{\rm N}_{\rm F336W,F438W}$ plane is entirely due to measurement errors, we adopt a procedure introduced by Anderson et al. (2009) and illustrated in Figure 7. In the left panel we show the $m_{\rm F814W}$ against $m_{\rm F475W} - m_{\rm F814W}$ CMD from Milone et al. (2012a). The red and blue lines superimposed on the CMD are the fiducials of the red and blue MSs and are drawn by hand. The verticalized $m_{\rm F814W}$ versus $\Delta^{\rm N}_{\rm F475W,\ F814W}$ diagram is plotted in the central panel, while the right panel shows $\Delta^{\rm N}_{\rm F275W,F814W}$ versus $\Delta^{\rm N}_{\rm F475W,\ F814W}$. Stars in common with this paper are marked with colored circles.

Photometry by Milone et al. (2012a) comes from ACS/WFC images, and hence represents a different data set than the WFC3 ones used in this paper. If the large $\Delta^{\rm N}_{\rm F275W,F814W}$ value for stars in the group A derived from UVIS/WFC3 photometry

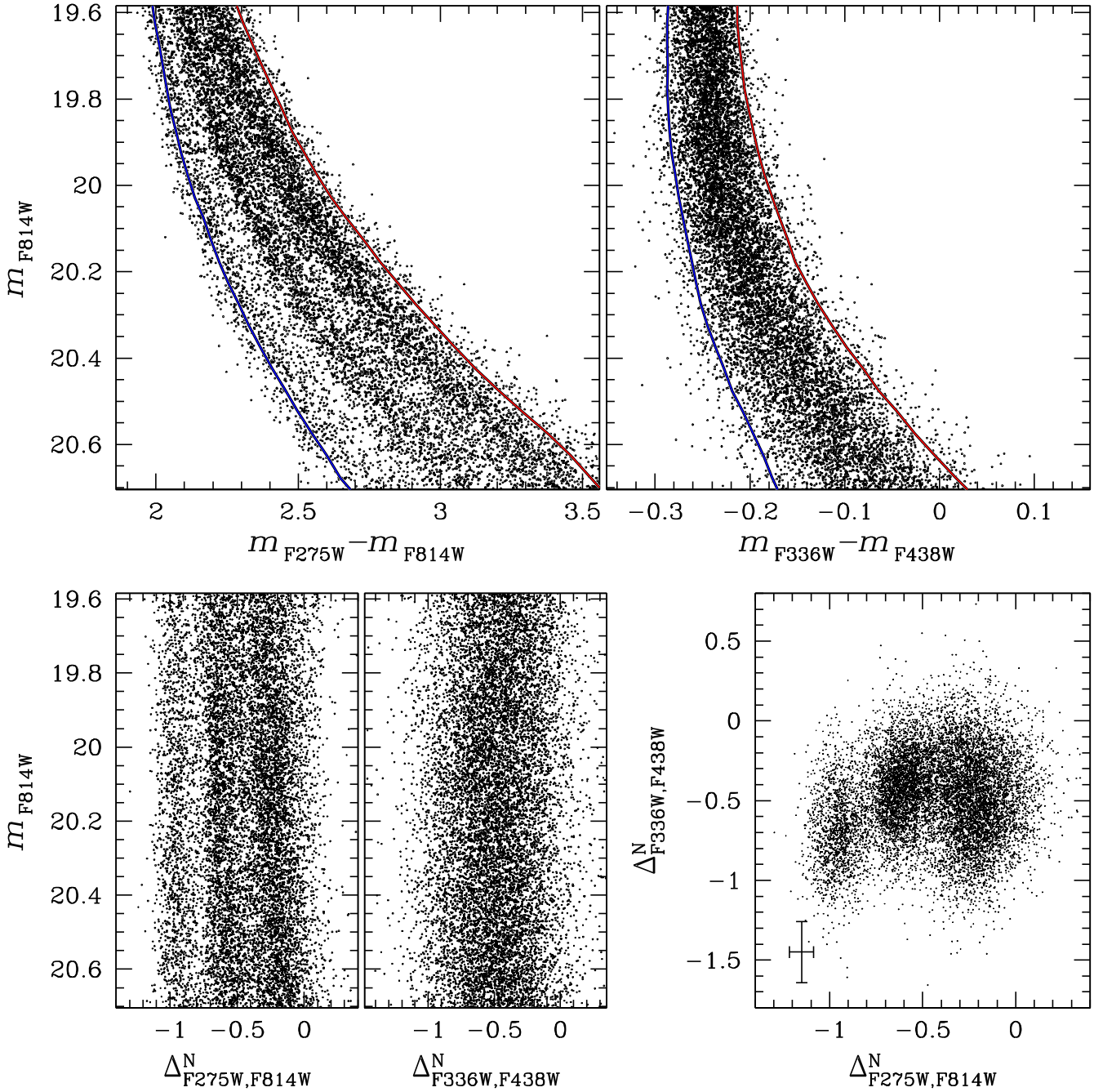

Figure 4. Upper panels: m_{F814W} vs. $m_{F275W} - m_{F814W}$ (left) and m_{F814W} vs. $m_{F336W} - m_{F438W}$ (right) CMD for MS stars in NGC 2808. The fiducials used to verticalize the RGB are represented by red and blue lines (see text for details). Lower panels: verticalized m_{F814W} vs. $\Delta^N_{F275W,F814W}$ (left) and m_{F814W} vs. $\Delta^N_{F336W,F438W}$ (middle) diagram for the stars in the upper panels. $\Delta^N_{F336W,F438W}$ is plotted against $\Delta^N_{F275W,F814W}$ in the lower-right panel.

is entirely due to photometric errors, then these stars have the same probability of having either small or large $\Delta^N_{F475W,\,F814W}$ derived from WFC/ACS. The systematically large $\Delta^N_{F475W,\,F814W}$ value of stars in group A, shown in the right panel of Figure 7, is evidence that they belong to a distinct stellar population.

3.3. Chemical Composition of Stellar Populations

Spectroscopy of RGB stars has revealed that NGC 2808 exhibits a very extended sodium–oxygen anticorrelation, with [O/Fe] spanning a range of more than 1 dex (Carretta et al. 2006). Twenty-seven stars analyzed by Carretta and collaborators are also included in our photometric sample, thus providing useful information on the chemical composition of the stellar populations we have identified in the previous sections. Carretta's stars are marked with large symbols in Figure 8 where we reproduce the $\Delta^N_{F336W,F438W}$ versus $\Delta^N_{F275W,F814W}$ diagram of Figure 3 (left panel), the Na–O anticorrelation from Carretta et al. (2006, middle panel), and the Mg–Al anticorrelation from Carretta (2014, right panel). Noticeably, stars in the B, C, D, and E stellar groups defined in this paper have almost the same iron content within ∼0.05 dex but populate different regions of the Na–O plane. The average elemental abundance for stars of population B, C, D,